

A digital PID controller for stabilizing large electric currents to the ppm level for Feshbach resonance studies

R. Thomas^{a)} and N. Kjærgaard^{b)}

Department of Physics, QSO-Centre for Quantum Science, and Dodd-Walls Centre, University of Otago, Dunedin, New Zealand

Magnetic Feshbach resonances are a key tool in the field of ultracold quantum gases, but their full exploitation requires the generation of large, stable magnetic fields up to 1000 G with fractional stabilities of better than 10^{-4} . Design considerations for electromagnets producing these fields, such as optical access and fast dynamical response, mean that electric currents in excess of 100 A are often needed to obtain the requisite field strengths. We describe a simple digital proportional-integral-derivative current controller constructed using a field-programmable gate array and off-the-shelf evaluation boards which allows for time-dependent control parameters, enabling optimal control of current sources with non-linear actuators. Our controller can stabilize an electric current of 340 A to the level of 2.4×10^{-6} with a control bandwidth of 2 kHz.

I. INTRODUCTION

Feshbach resonances are ubiquitous in the field of ultracold atomic physics¹ as they allow the interaction strength between atoms to be changed². This tunability can be used to explore effects such as the BEC-BCS phase transition in degenerate Fermi gases^{3–5}, Anderson localization⁶, and Efimov trimers^{7,8}. Sweeping a magnetic field across a Feshbach resonance is used to produce and study ultracold molecules^{9,10} which have complicated scattering properties^{11–13}. Feshbach resonances have also been critical in the study of dipolar quantum gases^{14–16}. Finally, Feshbach resonances can be used as a sensitive probe of variations in fundamental constants such as the ratio of electron to proton mass¹⁷.

Magnetic Feshbach resonances in alkali metal systems are typically accessed by using a pair of Helmholtz coils to generate stable fields ranging up to 1000 G. The required field stability, measured as the root-mean-square (RMS) fluctuations δB , is determined by two factors. The first is that $\delta B \ll |\Delta|$ where Δ is the width of the resonance which can range from 10 mG to 100 G¹. This level of stability is easily achieved for broad Feshbach resonances, but is more difficult for narrow resonances and especially resonances in non-zero angular momentum channels^{18,19}. The second factor is related to how one measures the magnetic field *in situ*; typically, the field is measured by probing the transition frequency between two magnetic sub-levels of trapped atoms using either Rabi or Ramsey spectroscopy. For both of these techniques, fluctuations in the transition frequency δf at a magnetic field B_0 corresponding to the Feshbach resonance need to satisfy $\delta f = \left. \frac{df}{dB} \right|_{B=B_0} \delta B \lesssim \Omega/(2\pi)$ where Ω is the Rabi frequency of the transition which is limited by the particular transition and available microwave or radio-frequency power. As a concrete example, consider the relatively broad Feshbach resonance between ⁸⁷Rb and ⁴⁰K atoms¹¹ located at $B_0 = 546$ G with width $\Delta = -3$

G and suppose a Rabi frequency of $\Omega = 2\pi \times 5$ kHz. If we require $\delta B \approx \Delta/20$, then the fractional stability $\delta B/B_0$ needed is about 270 ppm. However, calibration of the field at 546 G using radio-frequency spectroscopy of the least magnetically-sensitive transition in ⁴⁰K with $df/dB \approx 0.1$ MHz/G implies a needed magnetic field stability better than 100 ppm, so for this example the stability criterion for calibrating the field is stricter than the stability needed for using the resonance. As an alternate case, consider the relatively narrow Feshbach resonance between two ⁸⁷Rb atoms located at 1007 G with a width of 210 mG^{20,21}. Here, having $\delta B \approx \Delta/20$ implies a fractional stability of 10 ppm which is stricter than the 17 ppm stability needed for measurement using the least-sensitive transition.

In an experiment, one typically stabilizes the electric current generating the magnetic field and not the magnetic field itself. Design considerations for the Helmholtz coils, such as optical access, dynamic response, and heat removal mean that these coils are often large with few windings which means that currents in the hundreds of amperes are needed to produce magnetic fields in the 100 G – 1000 G range^{22–24}. Therefore, the task of stabilizing a large magnetic field to the level of 10 ppm is essentially equivalent to that of stabilizing a large (> 100 A) current to the same level, although further reductions in magnetic field noise can be achieved by measuring and stabilising the magnetic field directly²⁵. A typical solution is to build an analog proportional-integral-derivative (PID) feedback loop that stabilizes the current produced from a voltage-controlled power-supply using external regulating transistors to control the current. While some of these solutions have been very successful, with reported stabilities of better than 10 ppm^{23,26–30}, designing and implementing a high-precision, low-noise, and robust analog PID controller from discrete, linear components is a non-trivial task because the transistors used to regulate the current are inherently non-linear.

In this article, we present a digital PID controller that uses off-the-shelf components to regulate the electric current from a noisy (100 ppm) power supply. We achieve real-time performance by using a field-programmable gate array (FPGA) to measure the current, generate both a dynamic control signal and dynamic loop parameters,

^{a)}Electronic mail: ryan.j.thomas1@gmail.com

^{b)}Electronic mail: nk@otago.ac.nz

and implement the PID algorithm. The dynamic loop parameters are a key feature of our FPGA controller which makes it ideally suited for managing a non-linear system. Our system can stabilize a current of 340 A to the level of $795 \mu\text{A}_{\text{rms}}$ in a 13.7 kHz bandwidth, corresponding to a fractional magnetic field stability of 2.4 ppm.

II. IMPLEMENTATION

Single-input single-output control loops can be broken into four parts: a control value/set-point $r(t)$ for the state of the system, a measurement $y(t)$ of that state, an actuator signal $u(t)$ that affects the state, and a control law K that relates $u(t)$, $r(t)$, and $y(t)$ ³¹. At the heart of our control loop is a Xilinx Spartan 6 FPGA mounted on a commercial development board (Numato Labs Saturn) with 512 Mb of LPDDR RAM. As shown schematically in Fig. 1, the FPGA implements both the control law and the control signal in programmable logic, handles communication with the measurement and actuator electronics, stores measurement and control values in memory, and interfaces with a PC over a USB cable using the universal asynchronous receiver/transmitter (UART) protocol.

The physical system to be controlled is shown on the right-hand side of Fig. 1. A 15 V/440 A power supply (Agilent 6690A) sources the so-called “primary” current I_p that passes through a pair of Helmholtz coils and produces a magnetic field \mathbf{B} at the atoms in our experiment. The supply is set to voltage-controlled mode, and the value of I_p is controlled using three MOSFETs (IXYS IXFN200N07) connected in parallel with 25 mm x 5 mm copper bus bars. We connect transient voltage suppressing diodes (STMicroelectronics BZW50-47B) across the drain and source of each MOSFET to eliminate negative voltage spikes when the MOSFETs are turned off. The gate-source voltage of these transistors serves as the actuator signal $u(t)$ and changes the effective drain-source conductance which changes the primary current (inset of Fig. 1). The gate voltage is sourced by a high-precision, 20-bit digital-to-analog converter (DAC) mounted on a manufacturer-supplied evaluation board (Analog Devices EVAL-AD5791SDZ), and communication with the DAC uses the serial peripheral interface (SPI). The board is populated with nearly all the necessary components to produce a voltage in the range of -10 V to 10 V, and we use an external voltage reference (Maxim Integrated MAX6350) to supply the DAC with its 5 V reference.

We measure the primary current using a flux gate current transducer (Danisense IDSA600) which generates a secondary current $I_s = I_p/1500$ that passes through a precision 10Ω sense resistor (Vishay Y169010R0000T9L, 0.01% tolerance, 0.2 ppm/K) in the four-terminal Kelvin configuration to produce a sense voltage. We digitize this voltage to produce the measurement $y(t)$ using a low-noise, 24-bit, differential analog-to-digital converter (ADC) mounted on an evaluation board (Texas Instruments ADS127L01EVM). The evaluation board is already populated with the necessary components for proper functioning of the ADC such as a differential am-

plifier, low-noise voltage reference, and low-jitter 16 MHz clock, and we can communicate with it using SPI. The ADC uses a sigma-delta architecture and provides a number of different filters offering a trade-off between sampling rates and noise performance. For our work, we have found that using the low-latency filter with a sampling rate of 31.25 kSPS provides optimal results with a 3 dB bandwidth of 13.7 kHz and a noise floor of $2.74 \mu\text{V}_{\text{rms}}$ corresponding to $\delta I_p = 411 \mu\text{A}_{\text{rms}}$. The ADC has a voltage range of ± 2.5 V, corresponding to ± 375 A with our choice of transducer and sense resistor; however, the range can be changed easily with a different sense resistor. We store each measurement value in LPDDR memory which holds up to 4×10^6 values corresponding to over two minutes of continuous acquisition. This data can be retrieved from memory using the PC link for later analysis.

We realize our control law in programmable logic using a finite state machine that calculates a discrete approximation to the PID control law

$$u(t) = K_p e(t) + K_i \int_{-\infty}^t e(t') dt' + K_d \frac{de(t)}{dt} \quad (1)$$

where $e(t) = r(t) - y(t)$ is the error signal and K_p , K_i , and K_d are the proportional, integral, and derivative gain coefficients, respectively. The control signal $r(t)$ is either a piece-wise sequence of linear ramps generated on-the-fly using a linear-ramp generator or is an arbitrary, pre-programmed value read from memory. For each time step n separated in time by T_s (the inverse of the ADC sampling rate) we calculate the actuator value u_n as³¹

$$u_n = u_{n-1} + 2^{-N} A \left[\tilde{K}_p (e_n - e_{n-1}) + \frac{\tilde{K}_i}{2} (e_n + e_{n-1}) + \tilde{K}_d (e_n - 2e_{n-1} + e_{n-2}) \right] \quad (2)$$

where A is an overall conversion factor needed to account for the different discretization steps between a voltage measured by the ADC and one output by the DAC, and each of the \tilde{K} is the discrete equivalent of the PID gain coefficients in Eq. (1): $\tilde{K}_p = K_p$, $\tilde{K}_i = K_i T_s$, and $\tilde{K}_d = K_d T_s^{-1}$. Each \tilde{K} is represented as a 16-bit integer in programmable logic, and we approximate fractional gain values by shifting the sum of products right N bits, implementing division by 2^N . We take care with the order of operations in Eq. (2) as implemented in the FPGA so that values are not truncated prematurely and the full precision of the ADC is used.

We use the discrete control law in Eq. (2), which effectively calculates the correction to the actuator signal rather than the actuator signal itself, instead of the more direct discretization of Eq. (1) for two main reasons. The first is that the discrete integral term in Eq. (1) is unbounded, and one needs to include additional logic to prevent integral wind-up when either input or output values saturate. The second and more compelling reason is that our physical system is non-linear through the relationship between the MOSFET gate-source voltage and the drain-source conductance (inset of Fig. 1), and we need robust, low-noise control of currents from 20 A to 400 A. While

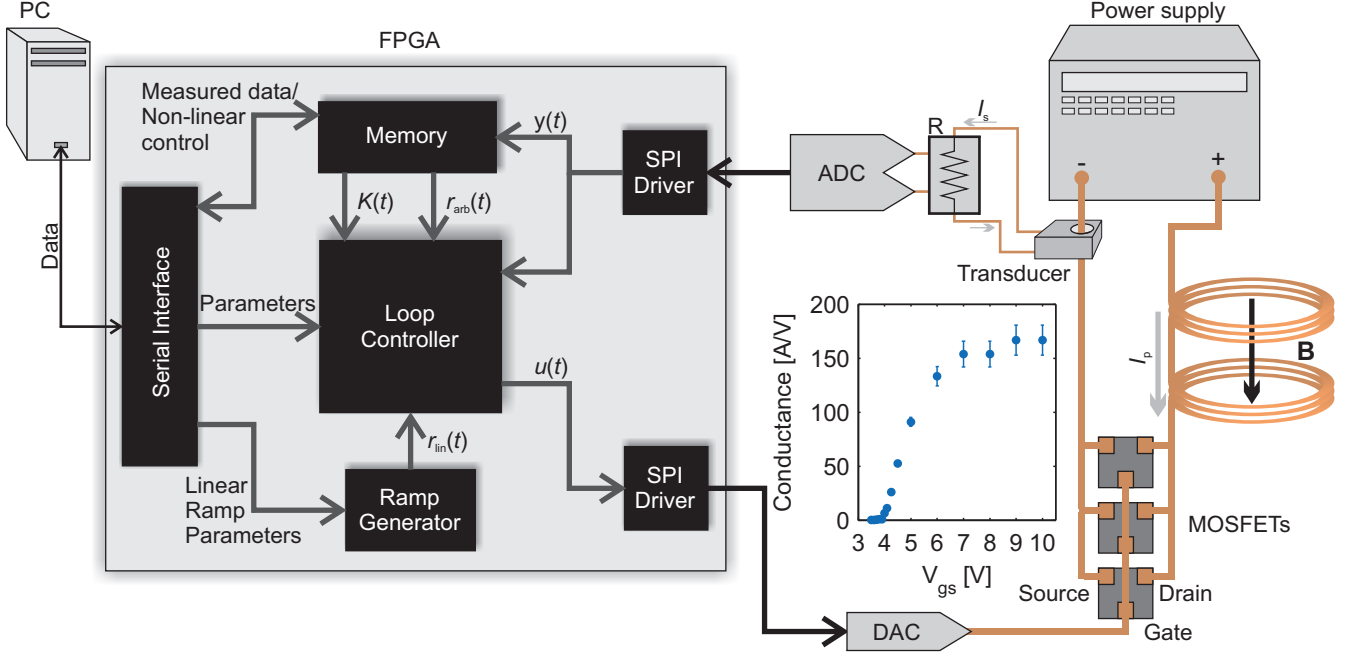


FIG. 1. Architecture of the PID controller as implemented in controllable logic and a diagram of the physical connections. The primary current I_p through a pair of Helmholtz coils is measured by using a fluxgate current transducer to produce a secondary current I_s that generates a voltage drop across a four-terminal precision resistor that is then digitized by an ADC. This measurement $y(t)$ is compared to either a linear control voltage $r_{lin}(t)$ or an arbitrary control voltage $r_{arb}(t)$, and an actuator value $u(t)$ is produced that is sent to a DAC. The loop controller uses either fixed loop parameters or a time-varying sequence of parameters $K(t)$ from memory. The voltage output of the DAC drives the gates of three of high-current MOSFETs that control the flow of I_p . A serial connection with a PC is used to set parameters and control voltages and to retrieve ADC measurements. Inset plot shows the drain-source conductance for a single MOSFET as a function of gate-source voltage.

we can approximate the dynamical relationship between $u(t)$ and $y(t)$ as linear over small intervals, this cannot be done over the entire range which crucially means that the optimum gain parameters for the controller change depending on the desired set-point $r(t)$. Therefore, at each time step we update u_n using not only the current and past values of the error signal but also according to pre-programmed values for each \tilde{K} corresponding to different values of the set-point r_n . Since Eq. (2) calculates the actuator signal as the sum of the previous value and a correction, it is easily adapted to include time-varying gain parameters. Equation (1), on the other hand, calculates the actuator anew at each time step, and changing the gain parameters between two different steps leads to significant jumps in the output signal due to the integral term.

III. TUNING AND MODELLING

In many implementations of PID controllers in experimental physics laboratories the gain coefficients are manually tuned in an iterative process to achieve the best possible performance. This technique is often used when either the performance simply needs to be “good enough”, or when measuring the system’s transfer function is not feasible. With our system, we can drive the MOSFET gate-source voltage with sinusoidal signals of varying frequencies ω , and, by changing the DC offset of these sig-

nals, we can measure the linearized AC system transfer function $G(\omega, I_p)$ about the steady-state DC primary current I_p corresponding to a particular DC gate-source voltage. Given a desired closed-loop response function $T(\omega)$, we calculate the appropriate control law $K(\omega, I_p)$ as³¹

$$\begin{aligned} K(\omega, I_p) &= \frac{T(\omega)}{1 - T(\omega)} G^{-1}(\omega, I_p) M^{-1}(\omega) \\ &= K_p(I_p) + \frac{K_i(I_p)}{i\omega} + i\omega K_d(I_p) \end{aligned} \quad (3)$$

$$G(\omega, I_p) \approx \frac{G_0(I_p)}{1 + \frac{i\omega}{\omega_1(I_p)} - \frac{\omega^2}{\omega_2^2(I_p)}}, \quad (4)$$

where we approximate the dynamical system represented by $G(\omega, I_p)$ as second order with set-point dependent coefficients $G_0(I_p)$, $\omega_1(I_p)$, and $\omega_2(I_p)$. To isolate the system response alone, we include the measurement response function $M(\omega)$ obtained from the ADC datasheet. Given a desired first-order closed-loop response $T^{-1}(\omega) = 1 + i\omega/\omega'$ with cut-off frequency ω' we determine the PID gain coefficients using

$$K_p(I_p) = \frac{\omega'}{G_0(I_p)\omega_1(I_p)} \quad (5a)$$

$$K_i(I_p) = \frac{\omega'}{G_0(I_p)} \quad (5b)$$

$$K_d(I_p) = \frac{\omega'}{\omega_2^2(I_p)G_0(I_p)}, \quad (5c)$$

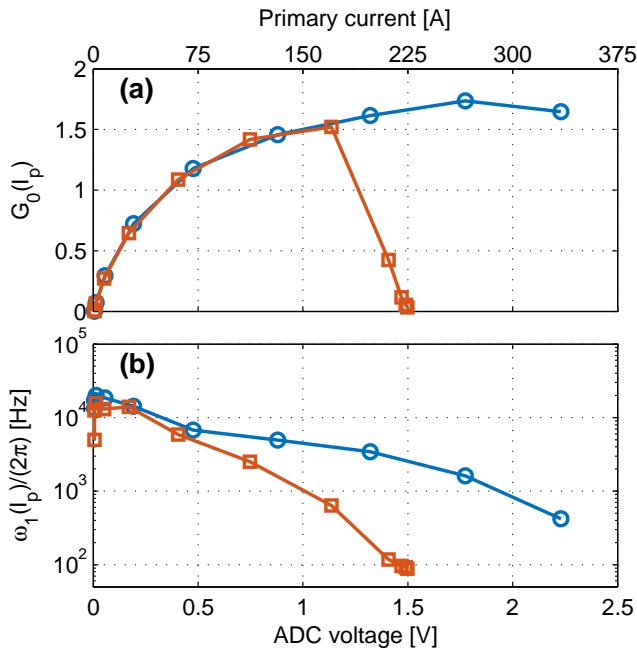


FIG. 2. System response as a function of ADC set-point for power supply voltages of 12.5 V (blue circles) and 7.2 V (red squares). (a) AC gain measured as the ratio of the voltage measured on the ADC and the driving voltage on the DAC. (b) First-order frequency $\omega_1/(2\pi)$.

where we have neglected the measurement response to simplify the calculation of the coefficients. This approximation is valid only when $\omega' \ll T_s^{-1}$.

Figures 2a and b show parameters $G_0(I_p)$ and $\omega_1(I_p)$ as functions of the steady-state primary current I_p for two different voltages 7.2 V and 12.5 V of the main power supply. The second-order frequency ω_2 is not shown because the additional term does not improve the model of the system response. The lack of data beyond an ADC voltage of 1.5 V ($I_p = 225$ A) for a power supply voltage of 7.2 V is simply due to the total resistance of our system which limits the maximum current to 225 A. For both power supply voltages we see a strong dependence of the system response on the desired primary current. In particular, we see how the AC gain $G_0(I_p)$ for a power supply voltage of 7.2 V drops precipitously between 150 and 225 A as the MOSFETs' conductances saturate (see inset of Fig. 1). This gain maximum, present also at the higher power supply voltage of 12.5 V, presents a problem when one needs to sweep the primary current across that peak. If the gain parameters are optimized for currents either before or after the gain peak then during the sweep the open-loop transfer function $K(\omega, I_p)G(\omega, I_p)$ will be larger than expected and the system may oscillate. Alternatively, if the gain parameters are optimized for the gain peak, then the controller will perform sub-optimally at currents where the AC gain is lower than its peak value. By adjusting the gain parameters with the desired primary current, we can ensure that we have an optimum loop response during the entire sweep.

Using the measured values of $G_0(I_p)$ and $\omega_1(I_p)$ in combination with Eq. (5) we program the controller to have a low-pass filter closed-loop response with various

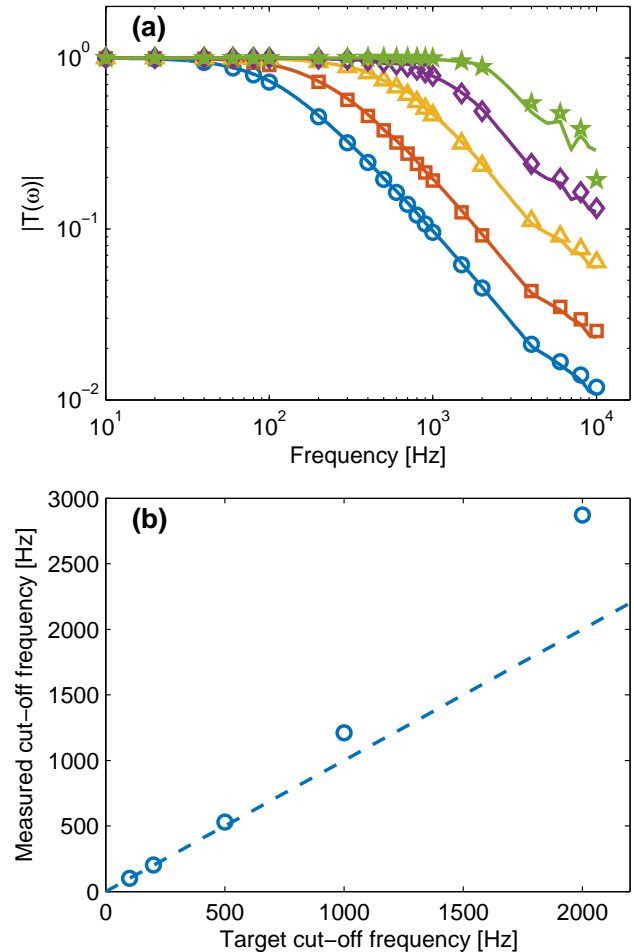


FIG. 3. Closed-loop response as a function of frequency for different desired low-pass filter frequencies with a power-supply voltage of 12.5 V. (a) Measured amplitude of the closed-loop response $|T(\omega)|$ at a set-point of $V_{\text{ADC}} = 1$ V for target frequencies of 100 Hz (circles), 200 Hz (squares), 500 Hz (triangles), 1 kHz (diamonds), and 2 kHz (stars). Solid lines are the prediction from the measured open-loop response and a model of the controller's behaviour. (b) Measured 3 dB cut-off frequency compared to the target cut-off frequency. Circles are the measurements, and the dashed line gives the ideal behaviour.

cut-off frequencies ω' ; the results are shown in Figs. 3a and b. To measure the closed-loop response we increase the current in the Helmholtz coils from 0 A to 150 A ($V_{\text{ADC}} = 1$ V) in 100 ms using a minimum-jerk trajectory³² to minimize transients before modulating the control signal with a sinusoidal signal of varying frequency and fixed amplitude of 20 mV which corresponds to a primary current amplitude of 3 A. We model the response by multiplying our measured $G(\omega, I_p)$ with $M(\omega)$ and the Fourier transform of Eq. (2). It is important to include both the latency of the ADC, equal to $T_s = 32$ μs , and the latency of the FPGA's PID process which comprises the time to read from the ADC (2.6 μs), the time to process the data (11 clock cycles, or 0.22 μs), the time to write to the DAC (2.6 μs), and the time for the DAC output to change (≈ 1 μs) for a total latency of ≈ 6 μs . Figure 3a shows that we get excellent

agreement between our measured response and the response expected from our model, with some deviations at high target cut-off frequencies. The actual cut-off frequencies, shown in Fig. 3b, differ significantly from the expected values for high cut-off frequencies, and this is a consequence of modelling the physical system as only a second-order dynamical system and neglecting the measurement response when calculating the gain coefficients. A more complete description would result in better correspondence between the desired and measured cut-off frequencies but would also require a more complex control law.

IV. PERFORMANCE

For our particular experiment, Feshbach resonance spectroscopy, we are primarily concerned with how much variability and noise there is in the current regulated by our controller when the set-point is fixed, and hence the variability in the magnetic field experienced by the atomic sample inside the Helmholtz coils. We are interested in both variations between experimental cycles and within a single cycle. Figure 4 shows how the current regulated by the device varies between experimental cycles. We increase the current from 0 A to the desired set-point in 100 ms using a minimum-jerk ramp and then hold the set-point steady for 400 ms, and each measurement is repeated ten times over the course of approximately three minutes. The loop parameters are set to give a nominal closed-loop response close to a 2 kHz low-pass filter although the real response is as shown in Fig. 3a. We find a cycle-to-cycle variation that is less than 1.3 mA for all current ranges and which decreases as the current is increased. The reason for this decrease is likely a result of changes in the open-loop response of the system: as the MOSFETs' conductances saturate they become less sensitive to higher-frequency perturbations which results in a lower overall noise. At our highest current, corresponding to 337.5 A, we measure an RMS variation of $795 \mu\text{A}_{\text{rms}}$ corresponding to a fractional stability of 2.4 ppm over the entire bandwidth (13.7 kHz) of the measurement.

In Fig. 5 we show the spectral characteristics of the steady state current signal for two different power-supply voltages under the same conditions as Fig. 4 for $V_{\text{ADC}} = 1$ V. In both cases noise is strongly suppressed below the nominal 2 kHz bandwidth of the controlled system. From 2 kHz to 6 kHz there is a broad noise plateau, and this is partly due to the ADC filter's latency of $T_s = 32 \mu\text{s}$. When $\omega T_s \ll 1$ the phase shift due to the filter latency does not significantly contribute to the overall phase shift of the system; however, when $\omega T_s \sim 1$ – which occurs at $\omega/(2\pi) \sim 5$ kHz – the latency of the filter limits the performance of the controller as a whole. For our system, our model predicts that at frequencies near 5 kHz our controller amplifies noise rather than suppressing it. This could potentially be improved with a higher sampling rate at a cost of more overall noise in the control loop. Noise peaks at ≈ 10 kHz and 12 kHz are due to external noise sources and are not inherent to the con-

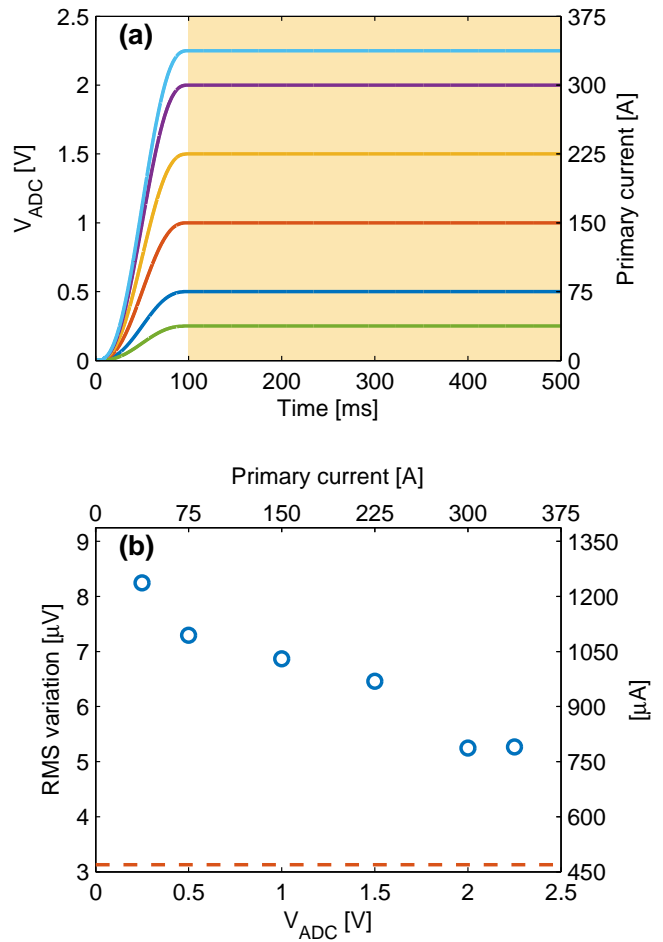


FIG. 4. Measuring the repeatability of the steady-state current across experimental cycles with a power-supply voltage of 12.5 V. (a) The temporal profile of the measured voltage/current for different steady-state set points. The shaded area indicates the temporal range where the control signal is constant. (b) The measured cycle-to-cycle RMS variation in measured ADC voltage (left axis) or primary current (right axis) as a function of set-point. The red, dashed line indicates the measured noise floor of the ADC and current transducer.

troller. By looking at the cumulative noise (Fig. 5b), we see that the controller can achieve sub-ppm levels of noise in bandwidths less than approximately 1.8 kHz.

Overall, using a lower power-supply voltage allows for control over the current with lower noise at a cost of a limited range of operation as shown in Fig. 2. However, the sharp drop in the AC gain at voltage set-points above 1 V requires that the controller's response be adjusted as the set-point changes. Figure 6 compares the effect of varying the loop response as a function of the set-point with a conventional fixed response. For the case of a fixed loop response, the loop gains were set to values appropriate for $V_{\text{ADC}} = 1.2$ V (the final steady-state value) and a 2 kHz closed-loop bandwidth. The variable-loop gains were calculated using Eq. (5) for the same bandwidth. As can be seen in Figs. 6a and b, the excessive gain as the current increases in the fixed response mode causes the system to oscillate. Additionally, the lack of gain at

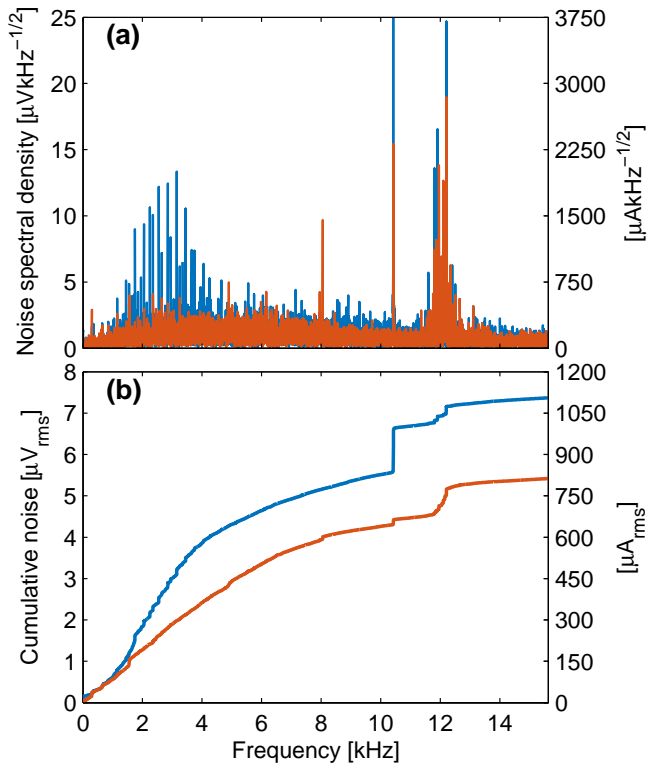


FIG. 5. Frequency-domain analysis of the error signal for power-supply voltages of 12.5 V (blue) and 7.2 V (red) for a steady-state set-point of $V_{\text{ADC}} = 1$ V ($I_p = 150$ A). The DC component has been removed for clarity. (a) Spectral density of the error signal. (b) Cumulative RMS noise in the error signal. Axes on the right give the equivalent quantities when converted to current.

the beginning of the current rise leads to a slow turn-on as the gate-source voltage slowly accumulates due to the integral term. Allowing the loop response to vary with the set-point eliminates oscillations during the initial ramp from 0 to 1.2 V and improves the initial turn-on behaviour.

Finally, we demonstrate that our system is capable of generating the required magnetic fields for Feshbach resonance studies. To measure the magnetic field, we first prepare a sample of ^{87}Rb atoms in a crossed-beam optical dipole trap and in the $|F = 2, m_F = 0\rangle$ state at a low field (9 G) using a separate, low-current power-supply. We then turn off the low-current supply and use our high-current system to increase the current from 0 A to a particular set-point in 75 ms using a minimum-jerk trajectory. We then wait for 50 ms for any transients to decay. At this point, we use Rabi spectroscopy of the $|F = 2, m_F = 0\rangle \rightarrow |F = 1, m_F = -1\rangle$ transition with a Rabi frequency of $\Omega/(2\pi) \approx 3$ kHz and a pulse time of $50 \mu\text{s}$ to determine the transition frequency from which we calculate the magnetic field. The results are shown in Fig. 7. We see that we get a highly linear relationship between the set-point and the measured magnetic field over an order of magnitude in magnetic field with a maximum uncertainty of 5 mG, making our system suitable for studying Feshbach resonances in a range of atomic systems.

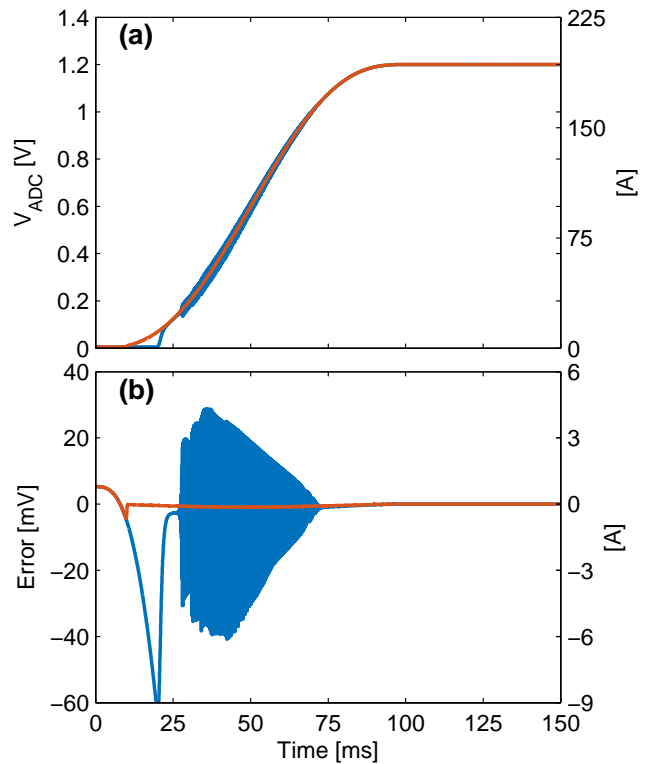


FIG. 6. Effect of varying the loop response with set-point. (a) Temporal profile of the measured voltage/current. Blue curve is without loop variation, red is with loop variation. (b) Difference between measured voltage/current and set-point without loop variation (blue) and with (red).

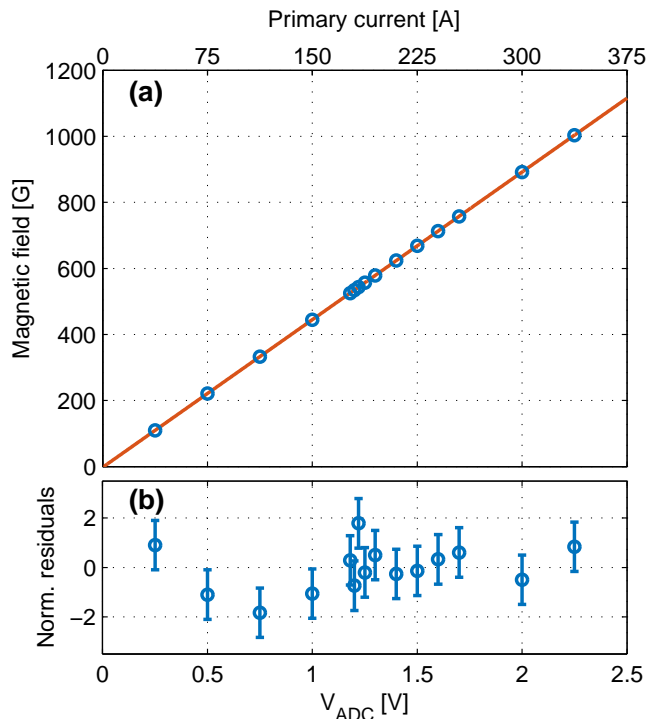


FIG. 7. Measurement of the magnetic field produced by our system as a function of voltage set-point. (a) Measured magnetic fields (blue circles) and linear fit (red line). Error bars are smaller than the width of the line. (b) Normalized residuals of the fit.

V. CONCLUSION

In this article we have presented a digital PID controller for stabilizing the large currents needed to generate magnetic fields for studies involving Feshbach resonances. The performance of our controller is easily tailored through a digitally programmable loop response which can be varied with the desired current, allowing for robust and precise control of non-linear systems. We achieve a fractional stability of 2.4 ppm in a 13.7 kHz bandwidth at 340 A.

We have already used our PID controller to study the behaviour of a Feshbach resonance in the collision of ^{87}Rb and ^{40}K atoms at energies far above threshold³³. Our system could be used for studying narrow Feshbach resonances at large magnetic fields, such as higher angular momentum Feshbach resonances or resonances in non-alkali metal systems³⁴, and it can also find use in other cold atom experiments such as ion trapping²⁵.

ACKNOWLEDGEMENTS

This work was funded by the New Zealand Tertiary Education Commission through the Dodd-Walls Centre for Photonic and Quantum Technologies.

SUPPLEMENTARY MATERIAL

See [supplementary material](#) for hardware definition language (HDL) code and Xilinx ISE 13.1 project files for the FPGA architecture used in this paper as well as MATLAB[®] software for controlling the FPGA from a computer. Documentation of the HDL and MATLAB[®] code is provided.

- ¹C. Chin, R. Grimm, P. Julienne, and E. Tiesinga, “Feshbach resonances in ultracold gases,” *Rev. Mod. Phys.* **82**, 1225–1286 (2010).
- ²S. Inouye, M. R. Andrews, J. Stenger, H.-J. Miesner, D. M. Stamper-Kurn, and W. Ketterle, “Observation of Feshbach resonances in a Bose-Einstein condensate,” *Nature* **392**, 151–154 (1998).
- ³M. Greiner, C. A. Regal, and D. S. Jin, “Emergence of a molecular Bose-Einstein condensate from a Fermi gas,” *Nature* **426**, 537–540 (2003).
- ⁴M. Bartenstein, A. Altmeyer, S. Riedl, S. Jochim, C. Chin, J. H. Denschlag, and R. Grimm, “Crossover from a molecular Bose-Einstein condensate to a degenerate Fermi gas,” *Phys. Rev. Lett.* **92**, 120401 (2004).
- ⁵T. Bourdel, L. Khaykovich, J. Cubizolles, J. Zhang, F. Chevy, M. Teichmann, L. Tarruell, S. J. J. M. F. Kokkelmans, and C. Salomon, “Experimental study of the BEC-BCS crossover region in lithium 6,” *Phys. Rev. Lett.* **93**, 050401 (2004).
- ⁶G. Roati, C. D’Errico, L. Fallani, M. Fattori, C. Fort, M. Zaccanti, G. Modugno, M. Modugno, and M. Inguscio, “Anderson localization of a non-interacting Bose-Einstein condensate,” *Nature* **453**, 895–898 (2008).
- ⁷T. Kraemer, M. Mark, P. Waldburger, J. G. Danzl, C. Chin, B. Engeser, A. D. Lange, K. Pilch, A. Jaakkola, H.-C. Nägerl, and R. Grimm, “Evidence for Efimov quantum states in an ultracold gas of caesium atoms,” *Nature* **440**, 315–318 (2006).
- ⁸S. Knoop, F. Ferlaino, M. Mark, M. Berninger, H. Schöbel, H.-C. Nägerl, and R. Grimm, “Observation of an Efimov-like trimer resonance in ultracold atom-dimer scattering,” *Nat. Phys.* **5**, 227–230 (2009).
- ⁹S. T. Thompson, E. Hodby, and C. E. Wieman, “Ultracold molecule production via a resonant oscillating magnetic field,” *Phys. Rev. Lett.* **95**, 1–4 (2005).
- ¹⁰C. A. Regal, C. Ticknor, J. L. Bohn, and D. S. Jin, “Creation of ultracold molecules from a Fermi gas of atoms,” *Nature* **424**, 47–50 (2003).
- ¹¹L. De Marco, G. Valtolina, K. Matsuda, W. G. Tobias, J. P. Covey, and J. Ye, “A degenerate Fermi gas of polar molecules,” *Science* **363**, 853–856 (2019).
- ¹²P. D. Gregory, M. D. Frye, J. A. Blackmore, E. M. Bridge, R. Sawant, J. M. Hutson, and S. L. Cornish, “Sticky collisions of ultracold RbCs molecules,” *Nat. Commun.* **10**, 3104 (2019).
- ¹³A. Christianen, M. W. Zwierlein, G. C. Groenenboom, and T. Karman, “Photoinduced two-body loss of ultracold molecules,” *Phys. Rev. Lett.* **123**, 123402 (2019).
- ¹⁴I. Ferrier-Barbut, H. Kadau, M. Schmitt, M. Wenzel, and T. Pfau, “Observation of Quantum Droplets in a Strongly Dipolar Bose Gas,” *Phys. Rev. Lett.* **116**, 1–6 (2016).
- ¹⁵T. Lahaye, J. Metz, B. Fröhlich, T. Koch, M. Meister, A. Griesmaier, T. Pfau, H. Saito, Y. Kawaguchi, and M. Ueda, “d-wave collapse and explosion of a dipolar Bose-Einstein condensate,” *Phys. Rev. Lett.* **101**, 080401 (2008).
- ¹⁶T. Koch, T. Lahaye, J. Metz, B. Fröhlich, A. Griesmaier, and T. Pfau, “Stabilization of a purely dipolar quantum gas against collapse,” *Nat. Phys.* **4**, 218–222 (2008).
- ¹⁷C. Chin and V. V. Flambaum, “Enhanced sensitivity to fundamental constants in ultracold atomic and molecular systems near Feshbach resonances,” *Phys. Rev. Lett.* **96**, 230801 (2006).
- ¹⁸Y. Cui, C. Shen, M. Deng, S. Dong, C. Chen, R. Lü, B. Gao, M. K. Tey, and L. You, “Observation of broad d-wave Feshbach resonances with a triplet structure,” *Phys. Rev. Lett.* **119**, 203402 (2017).
- ¹⁹X.-C. Yao, R. Qi, X.-P. Liu, X.-Q. Wang, Y.-X. Wang, Y.-P. Wu, H.-Z. Chen, P. Zhang, H. Zhai, Y.-A. Chen, and J.-W. Pan, “Degenerate Bose gases near a d-wave shape resonance,” *Nat. Phys.* **15**, 570–576 (2019).
- ²⁰T. Volz, S. Dürr, S. Ernst, A. Marte, and G. Rempe, “Characterization of elastic scattering near a Feshbach resonance in ^{87}Rb ,” *Phys. Rev. A* **68**, 010702 (2003).
- ²¹S. Dürr, T. Volz, and G. Rempe, “Dissociation of ultracold molecules with Feshbach resonances,” *Phys. Rev. A* **70**, 031601 (2004).
- ²²D. O. Sabulsky, C. V. Parker, N. D. Gemelke, and C. Chin, “Efficient continuous-duty bitter-type electromagnets for cold atom experiments,” *Rev. Sci. Instrum.* **84**, 104706 (2013).
- ²³T. Luan, T. Zhou, X. Chen, and Z. Ma, “A modified bitter-type electromagnet and control system for cold atom experiments,” *Rev. Sci. Instrum.* **85**, 024701 (2014).
- ²⁴K. Roux, B. Cilenti, V. Helsen, H. Konishi, and J. P. Brantut, “Compact bulk-machined electromagnets for quantum gas experiments,” *SciPost Phys.* **6**, 48 (2019).
- ²⁵B. Merkel, K. Thirumalai, J. E. Tarlton, V. M. Schfer, C. J. Ballance, T. P. Harty, and D. M. Lucas, “Magnetic field stabilization system for atomic physics experiments,” *Rev. Sci. Instrum.* **90**, 044702 (2019).
- ²⁶A. Marte, *Feshbach-Resonanzen bei Stößen ultrakalter Rubidiumatome*, PhD thesis, Technische Universität München (2003).
- ²⁷A. Trenkwalder, *Creation of a Strongly Interacting Fermi-Fermi Mixture of ^6Li and ^{40}K* , PhD thesis, University of Innsbruck (2011).
- ²⁸L. J. Wacker, *Few-body physics with ultracold potassium rubidium mixtures*, PhD thesis, Aarhus University (2015).
- ²⁹X.-T. Xu, Z.-Y. Wang, R.-H. Jiao, C.-R. Yi, W. Sun, and S. Chen, “Ultra-low noise magnetic field for quantum gases,” *Rev. Sci. Instrum.* **90**, 054708 (2019).
- ³⁰Y.-M. Yang, H.-T. Xie, W.-C. Ji, Y.-F. Wang, W.-Y. Zhang, S. Chen, and X. Jiang, “Ultra-low noise and high bandwidth bipolar current driver for precise magnetic field control,” *Rev. Sci. Instrum.* **90**, 014701 (2019).
- ³¹J. Bechhoefer, “Feedback for physicists: A tutorial essay on control,” *Rev. Mod. Phys.* **77**, 783–836 (2005).
- ³²C. S. Chisholm, R. Thomas, A. B. Deb, and N. Kjærgaard, “A three-dimensional steerable optical tweezer system for ultracold atoms,” *Rev. Sci. Instrum.* **89**, 103105 (2018).

³³R. Thomas, M. Chilcott, E. Tiesinga, A. B. Deb, and N. Kjærgaard, “Observation of bound state self-interaction in a nano-eV atom collider,” *Nat. Commun.* **9**, 4895 (2018).

³⁴V. Barbé, A. Ciamei, B. Pasquiou, L. Reichsöllner, F. Schreck, P. S. Żuchowski, and J. M. Hutson, “Observation of Feshbach resonances between alkali and closed-shell atoms,” *Nat. Phys.* **14**, 881–884 (2018).